A Wavelet-based Variability Model (WVM) for Solar PV Power Plants

Matthew Lave, Jan Kleissl, Joshua S. Stein

Abstract – **A wavelet variability model (WVM) for simulating solar photovoltaic (PV) power plant output given a single irradiance point sensor timeseries using spatio-temporal correlations is presented. The variability reduction (VR) that occurs in upscaling from the single point sensor to the entire PV plant at each timescale is simulated, then combined with the wavelet transform of the point sensor timeseries to produce a simulated power plant output. The WVM is validated against measurements at a 2MW residential rooftop distributed PV power plant in Ota City, Japan and at a 48MW utility-scale power plant in Copper Mountain, NV. The WVM simulation match the actual power output well for all variability timescales, and the WVM compares well against other simulation methods.**

Index Terms–**PV, Solar, Upscaling, Wavelets, Geographic Dispersion, Variability.**

I. INTRODUCTION

High penetration of solar power is highly desirable from an environmental point of view, but the variability of solar photovoltaic (PV) power is considered an obstacle to managing the electrical distribution and transmission system. Solar PV power production is variable due to the rising and setting of the sun, cloud shadows, changes in composition of the clear atmosphere (e.g., dust, smoke, humidity), and system-specific variables such as inverter performance, module temperature, and soiling. Cloud-induced fluctuations have the highest potential to affect the electric grid since they introduce changes in power production at short timescales (<1-hr). The other causes of variability typically change over longer timescales (>1-hr) and are often more predictable than clouds. Fortunately, though, since clouds are not homogeneous, geographic smoothing reduces short timescale variability for a fleet of PV systems.

We define the variability reduction (VR) as the ratio of variance in a time-varying quantity (e.g., normalized irradiance or PV power output) at one site to the variance of the average of all sites in a network (i.e., a PV power plant). Defined this way, an increase in VR will indicate a decrease in the aggregate variability. Values of VR depend on the correlation between sites: $VR = 1$ for perfectly correlated sites and $VR = N$ for independent sites. VR values of 2.8 for 1-min irradiance timeseries of 9 sites in a 4 km by 4 km grid in Tsukuba, Japan [1], 1.7 to 3.3 for 1-min steps of power output of 3 sites in 100s of km apart in Arizona [2], 2.4 to 4.1 for 5-min clear-sky index timeseries of 4 sites 100s of km apart in Colorado [3], and 2.7 for 5-min power output of 100 sites spread throughout Germany [4] have been found.

Other studies have shown the decorrelation of PV system output as a function of distance [5-7]. Hoff and Perez [8] showed that the correlation values collapse onto a line when the distance is divided by timescale. Accounting for cloud speed as determined from satellite further decreased the scatter, suggesting a universal correlation law.

With a similar objective to the present study, Marcos et al. [9] used a solar irradiance point sensor timeseries to simulate variability of a larger power plant using a transfer function based on a low pass filter which is scaled by the power plant area. Here, we describe a wavelet variability model that will help system planners gain an understanding of the variability of a potential power plant (i.e., largest ramp rates and how often they occur) with only limited data required as input. We describe the steps of the model in section II, section III demonstrates and validates use of the model at two test sites, and section IV presents the conclusions.

II. METHODS

We propose a wavelet variability model (WVM) for simulating power plant output given (1) measurements from a single irradiance point sensor, (2) knowledge of the power plant footprint and PV density (Watts of installed capacity per m^2), and (3) a correlation scaling coefficient (section IIC) by determining the geographic smoothing that will occur over the area of the plant (Fig. 1). The simulated power plant may have any density of PV coverage: it may be distributed generation (i.e., a neighborhood with rooftop PV) with low PV density, centrally located PV as in a utility-scale power plant with high PV density, or any combination of both. In the WVM, we assume a statistically invariant irradiance field both spatially and in time over the day (i.e., stationary), and we assume that correlations between sites are isotropic: they depend only on distance, not direction.

M. Lave is with the Mechanical and Aerospace Engineering Department at the University of California, San Diego, CA 92093 (e-mail: mlave@ucsd.edu), and Sandia National Laboratories, Albuquerque, NM, 87123 (e-mail: mlave@sandia.gov).

J. Kleissl is with the Mechanical and Aerospace Engineering Department at the University of California, San Diego, CA 92093 (e-mail: jkleissl@ucsd.edu).

J. Stein is with Sandia National Laboratories, Albuquerque, NM, 87123 (e-mail: jsstein@sandia.gov).

WVM Inputs

PV Plant Footprint

Density of PV

Point Sensor Timeseries

Location/Day Dependent "A" Coefficient

determine variability reduction (smoothing) at each wavelet timescale

WVM Outputs

Plant Areal Average Irradiance
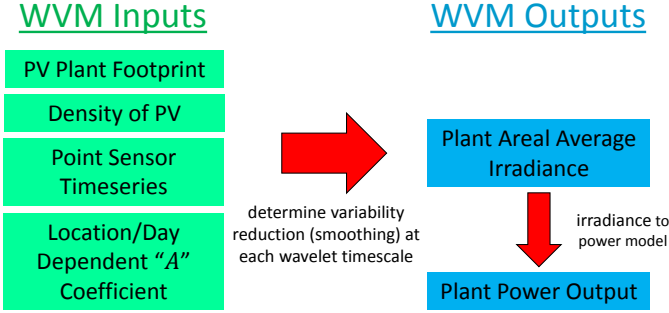
irradiance to power model

Plant Power Output

Fig. 1. Diagram showing the inputs and outputs for the WVM.

The WVM is designed to provide simulated power plant output to grid integration studies which test the effects of adding PV to existing electric feeders. These studies are done historically, after load and irradiance have been measured, and show the potential impacts of PV variability had PV been installed on the feeder being studied.

While the WVM is not a stand-alone forecasting model, it could be integrated into forecasting methods if spatially-distributed forecasted irradiances were available at high temporal resolution. However, satellite and numerical weather prediction forecast models typically only output at a temporal resolution of 30 minutes such that an upscaling method such as the WVM is not required since essentially no geographic smoothing occurs over power plant length scales (O~10 km) at such long timescales.

The main steps to the WVM are detailed in the sections below.

A. Wavelet Decomposition

We decompose the input irradiance point sensor timeseries into its components at various timescales by using a wavelet transform.

To obtain a stationary signal, the irradiance timeseries is normalized such that output during clear conditions is 1.

$$GHI_{norm}(t) = GHI(t)/GHI_{clr}(t), \qquad (1)$$

where $GHI_{norm}(t)$ is the normalized signal, and $GHI_{clr}(t)$ is the clear-sky model (here the Ineichen model [10]). For simplicity of notation, we here assume that the point sensor is a global horizontal irradiance (GHI) sensor. If instead a plane of array (POA) sensor were used, a POA clear-sky model would be required.

The wavelet transform of the clear-sky index, $GHI_{norm}(t)$, is:

$$w_{\bar{t}}(t) = \int_{t_{start}}^{t_{end}} GHI_{norm}(t') \frac{1}{\sqrt{\bar{t}}} \psi\left(\frac{t'-t}{\bar{t}}\right) dt', \qquad (2)$$

where the wavelet timescale (duration of fluctuations) is $\bar{t}$, t_{start} and t_{end} designate the start and end of the GHI timeseries, and t' is a variable of integration. For the discrete wavelet transform, $\bar{t}$ is increased by factors of 2, such that values of $\bar{t}$ are defined by $\bar{t} = 2^j$. We used the top hat wavelet, defined by:

$$\psi(T) = \begin{cases} 1, & \frac{1}{4} < T < 3/4 \\ -1, & 0 < T < \frac{1}{4} \quad || \quad \frac{3}{4} < T < 1, \\ 0, & else \end{cases} \qquad (3)$$

because of its simplicity and similarity to the shape of solar power fluctuations [11]. For 1-day at 1-sec resolution, we compute wavelet modes (timeseries) for $\bar{t}$ values ranging from 2-sec ($j = 1$) to 4096-sec ($j = 12$), thus decomposing the $GHI_{norm}(t)$ timeseries into 12 modes $w_{\bar{t}}(t)$ showing fluctuations at these various timescales. Symmetric signal extension is used to ensure resolution at endpoints. The largest timescale over which correlations are considered is 4096 sec ($j = 12$) because over the spatial scales of interest (O~10 km) the amount of smoothing that occurs at longer time scales is insignificant. In addition, modes for $j > 12$ require such significant signal extension that they are no longer representative of true fluctuations in the irradiance timeseries. We adopt a special definition for the highest wavelet mode, defining $w_{\bar{t}=2^{12}}(t)$ to be the moving average with window 4096-sec. By doing so, we achieve the property that the sum of all wavelet modes equals the original input signal:

$$\sum_{j=1}^{12} w_{\bar{t}=2^j}(t) = GHI_{norm}(t). \qquad (4)$$

B. Distances

We next discretize the power plant into individual 'sites'. A single site is chosen to be an area over which $\rho(d_{m,n}, \bar{t}) \approx 1$ for the timescales of interest. For distributed plants, a single site is one rooftop PV system. For utility-scale plants, a single site is a small container of PV modules, as dictated by computational limitations. When using larger containers, a correction is applied for the in-container smoothing. Once discrete sites have been defined, the distance between each pair of sites is computed.

C. Correlations

To determine correlations between sites we assume that correlation is a function of distance divided by timescale [8]:

$$\rho(d_{m,n}, \bar{t}) = \exp(-\frac{1}{A}\frac{d_{m,n}}{\bar{t}}), \qquad (5)$$

where ρ is the correlation between sites, $d_{m,n}$ is the distance between sites m and n, $\bar{t}$ is the timescale, and A is a correlation scaling factor. The A value can be found using a small network of irradiance sensors (at least ~4-6 sites) where the correlations, distances, and timescales are known and A may be solved for using Eq. 5. The A value varies day-by-day and by location due to changing cloud speed. Smaller A values (1-3, typically observed at coastal sites with low, slow clouds) result in lower correlations between sites, while large A values (>4, typical of inland sites with high, fast-moving clouds) mean higher correlations. Through future work, we will create a closed form solution where A can be determined from geographic and meteorological variables and multiple irradiance sensors are not required.

D. Variability Reduction

The variability reduction as a function of timescale, $VR(\bar{t})$, is defined as the variance of the point sensor divided by the variance of the entire PV power plant at each timescale. VR can be expressed as the inverse of the average of all correlations modeled in Eq. (5):

$$VR(\bar{t}) = \frac{N^2}{\sum_{m=1}^{N}\sum_{n=1}^{N}\rho(d_{m,n},\bar{t})}, \qquad (6)$$

where N is the total number of sites. Defined this way, $VR = N$ for entirely independent sites ($\rho = 0, m \neq n$), and $VR = 1$ for entirely dependent sites.

E. Simulate Wavelet Modes of Power plant

By combining the wavelet modes $w_{\bar{t}}(t)$ found in section II.A with the variability reductions $VR(\bar{t})$ from section II.D, we simulate the wavelet modes of the power plant. The simulated wavelet modes of normalized power are reduced in magnitude by the square root of VR:

$$w_{\bar{t}}^{sim}(t) = \frac{w_{\bar{t}}(t)}{\sqrt{VR(\bar{t})}}, \qquad (7)$$

where $w_{\bar{t}}^{sim}(t)$ are the simulated power plant wavelet modes. We can sum the simulated wavelet modes (inverse wavelet transform) to create a simulated clear-sky index of area-averaged GHI over the power plant:

$$< GHI_{norm}^{sim} >_{pp}(t) = \sum_{j=1}^{12} w_{\bar{t}=2^j}^{sim}(t). \qquad (8)$$

F. Convert to Power Output

Power output is obtained by multiplying the spatially averaged irradiance (section II.E) by a clear-sky power output model, $P(t)_{clr}$.

$$P(t)^{sim} = < GHI_{norm}^{sim} >_{pp}(t) * P(t)_{clr} \qquad (9)$$

$P(t)_{clr}$ is created by combining a plane of array irradiance clear-sky model with the plant's capacity, PC, and a constant conversion factor, C.

$$P(t)_{clr} = PC \times C \times POI_{clr}(t) \qquad (10)$$

To obtain $POI_{clr}(t)$, we apply the Page Model [12] to $GHI_{clr}(t)$. Since the Page Model requires GHI and diffuse irradiance as inputs, diffuse fraction was estimated as in [13]. The constant conversion factor, C, is determined based on the power plant's conversion efficiency.

Since PV plant power output is nearly linearly proportional to spatially averaged irradiance [14], using only a constant multiplier (C) is a reasonable approximation for this application. In practice, though, more sophisticated performance models [15] should be used that depend on ambient temperature, wind speed, and module specifications. The improvement in accuracy of power output achieved by using such a non-linear model depends on how far variables such as temperature deviate from standard test conditions (STC), but is expected to usually be less than 10%. Errors in estimating the variability at short timescales will be even smaller, since most of the non-linear irradiance to power effects occur over long timescales.

III. RESULTS/APPLICATION TO OTA CITY AND COPPER MOUNTAIN POWER PLANTS

To demonstrate the WVM model, we use the 2.13MW$_p$ distributed generation (residential rooftop) plant in Ota City, Japan, and the Copper Mountain 48MW$_p$ utility scale PV power plant in Boulder City, NV. Footprints of each plant are shown in Fig. 2. For both, the results of the WVM simulation were compared to the actual measured power output for the whole plant.

The Ota City (OC) plant consists of 550 houses, most with polycrystalline silicon PV systems ranging from 3-5kW, at varying tilts and azimuths. The average orientation of all PV modules producing power at OC on the test day was found to be 15° tilt from horizontal and 10° azimuth east of south.

GHI recorded once per second using an EKO instruments ML-020VM silicon pyranometer (expected uncertainty$< 5\%$) was used as input to the WVM, and power output of the entire neighborhood also at 1-sec resolution was used for validation. The total power output was simply the sum of the output of
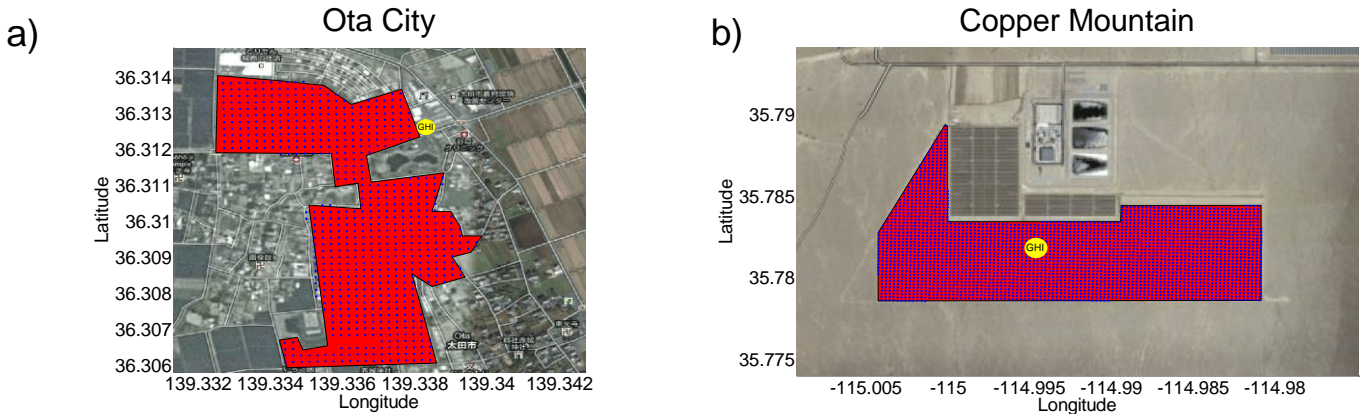

Fig. 2. Polygons showing the footprints of the (a) Ota City and (b) Copper Mountain power plants. The red shading shows the polygon footprints, while the blue dots show the simulation containers representing either houses (Ota City), or small groups of PV modules (Copper Mountain). The large yellow dots indicate the location of the GHI point sensors used as input. The Ota City map shows approximately 1×1 km, while the Copper Mountain map is approximately 3×2 km. Maps © Google Maps.
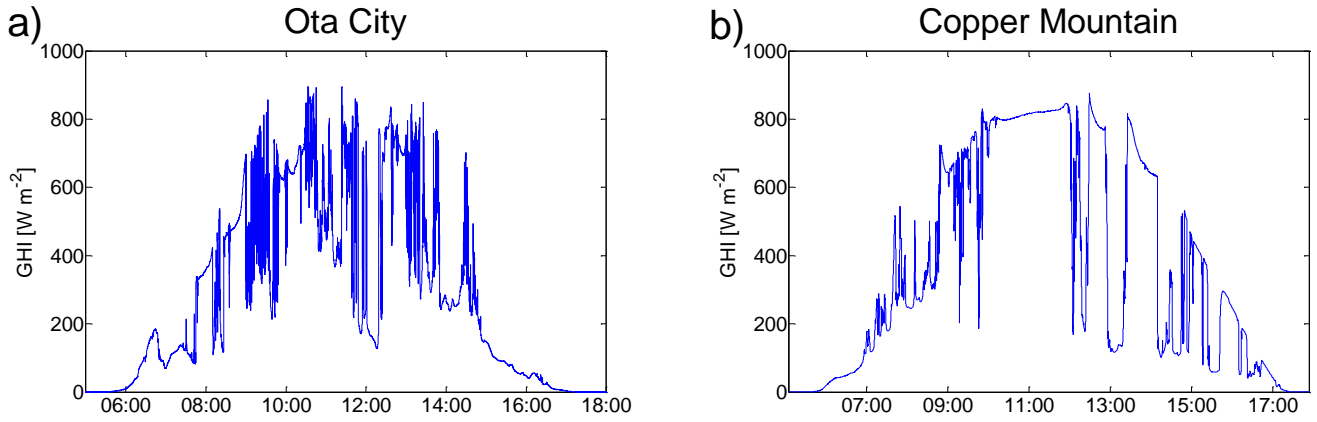
Fig. 3. GHI at 1-sec resolution at (a) Ota City on October 12th, 2007, and at (b) Copper Mountain on October 1, 2011. X-axis is time in [HH:MM].

each house, so ignored transmission losses. Results for a typically variable day (October 12, 2007) in OC (Fig. 3a) will be presented.

The Sempra Generation Copper Mountain (CM) plant contains ground-mounted cadmium telluride (CdTe) thin-film PV at a fixed tilt of 25°. GHI at 1-sec resolution from a Kipp & Zonen CMP11 (expected daily uncertainty < 2%) was input to the WVM model, and the output was compared to power output of the entire plant also measured at 1-sec. Total power output was the sum of all inverter power outputs, so ignores AC transmission losses. October 1, 2011 was chosen as a typically variable test day at CM (Fig. 3b).

For purposes of validating the WVM, we will use irradiances at a point, area-averaged irradiances, and power output (for nomenclature see Table 1). For validation, the simulated power output (P^{sim}) is compared to the actual power output (P). The point sensor is included in some comparisons to show how the WVM output has improved from the input GHI.

Table 1: Nomenclature for GHI, simulated power output, and actual power output. Angle brackets denote averaging. GHI_{norm} is the clear-sky index, while $< GHI_{norm} >_{pp}$ is the ratio of actual to clear-sky output power. Since the later does not align with the definition of the clear-sky index, the GHI_{norm} notation was chosen.

	GHI units [W m⁻²]	Clear-sky index [-]	Power units [MW]
measured point sensor	GHI	GHI_{norm}	
simulated power plant output	$< GHI^{sim} >_{pp}$	$< GHI^{sim}_{norm} >_{pp}$	P^{sim}
actual power plant output	$< GHI >_{pp}$	$< GHI_{norm} >_{pp}$	P

A. Inputs and Running the Model

The layouts of OC and CM were input and the WVM picked discrete points inside these footprints to use as "sites" in the simulation, as shown in Fig. 2. The spacing of sites was chosen based on the density of the plant. For OC, discrete sites were spaced roughly 20m apart such that each site represented a single house with rooftop PV. For CM, sites were closer together (a few meters), with each site representing a sufficiently small group of PV modules that can be assumed to have a correlation coefficient of 1.
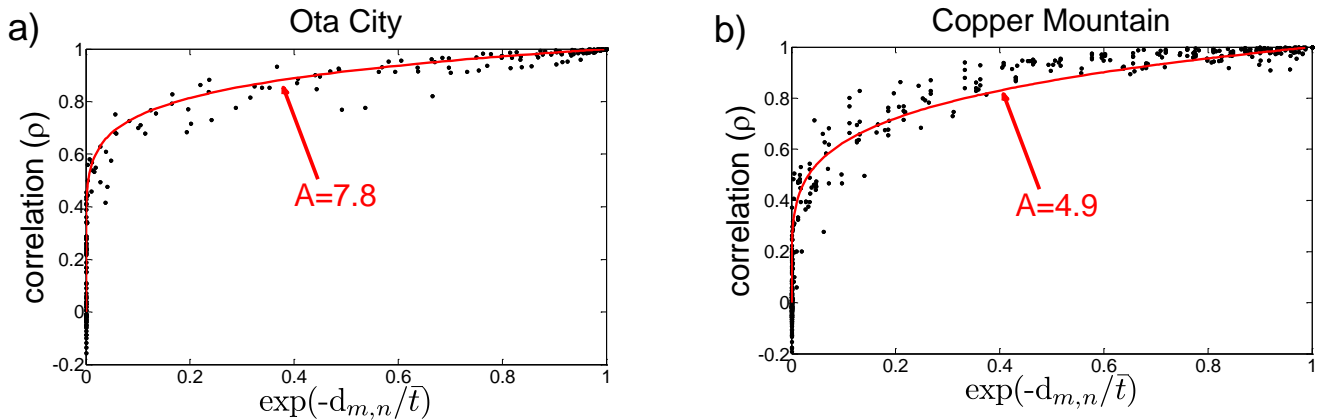

Fig. 4. Correlations of wavelet modes for pairs of point sensors (a) at Ota City on October 12th, 2007 and (b) Copper Mountain on October 1, 2011. The x-axis is $\exp(-\frac{d_{m,n}}{\bar{t}})$ to show the exponential relationship between correlation and the quantity distance divided by timescale. Six GHI point sensors were used at Ota City, and 15 plane-of-array reference cells were used at Copper Mountain. Time scales range from 2-sec to 2048-sec. Dots to the far left have large $\frac{d_{m,n}}{\bar{t}}$ ratios meaning either very short timescales or very long distances, while dots to the far right have small $\frac{d_{m,n}}{\bar{t}}$ ratios so either very long timescales or very short distances. The red line is the line of best fit and corresponds to using $A = 7.8$ (Ota City) or $A = 4.9$ (Copper Mountain) in Eq. 5.
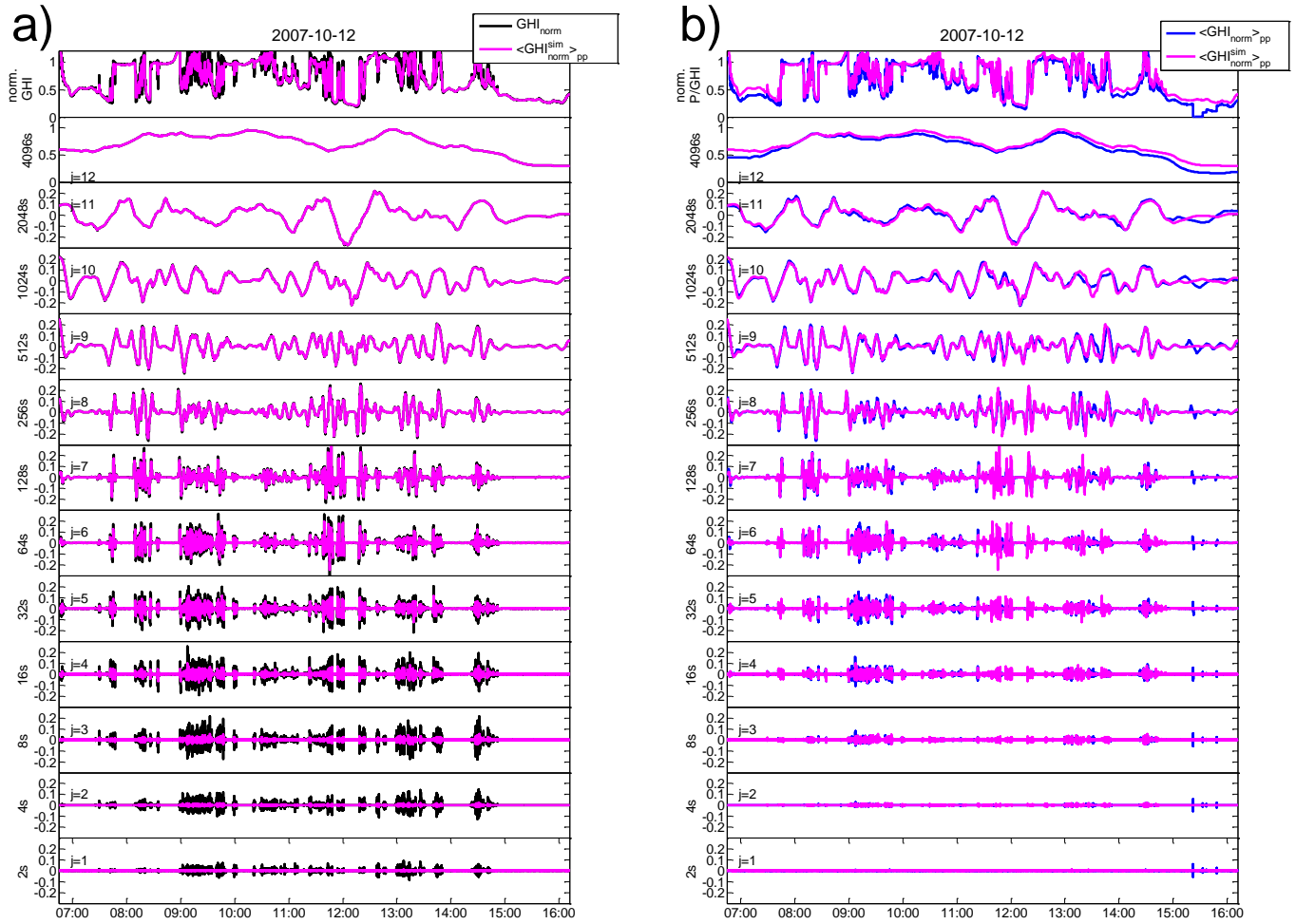
Fig. 5. [top most plots] Clear-sky index timeseries, and [bottom 12 plots] wavelet modes for Ota City on the test day. [Left] Clear-sky index measured (GHI_{norm}, black) and simulated spatially averaged across the power plant ($< GHI^{sim}_{norm} >_{pp}$, magenta). [Right] Power plant output 'clear-sky index' measured ($< GHI_{norm} >_{pp}$, blue) and simulated ($< GHI^{sim}_{norm} >_{pp}$, magenta).

Also input to the WVM were the GHI measurement vectors, as well as latitude, longitude, and UTC offset (for creating the clear-sky model, GHI_{clr}). The test day at OC contains large cloud-induced irradiance fluctuations throughout the day. The test day at CM has some large irradiance fluctuations as well as a few clear periods (e.g., 10:00-12:00). Thus, the WVM model will be tested at two different sites and types of daily cloud conditions (highly variable and partly variable).

For OC on the test day, $A = 7.8$, as found from 6 GHI point sensors. Similarly, 15 plane-of-array reference cells at CM were used to determine $A = 4.9$ on October 1 (Fig. 4). The small scatter of correlation points (black dots) around the best-fit curve, most noticeable at CM, is likely due to small anisotropic effects (i.e., pairs of sensors arranged in a certain direction may have higher correlation for all timescales).

Following steps A-E (section II), a simulated normalized irradiance (similar to a clear-sky index, see Table 1) timeseries for the entire Ota City and Copper Mountain power plants was created, $< GHI^{sim}_{norm} >_{pp} (t)$. Fig. 5a shows the effect of spatial averaging on the (simulated) reduction in variability.

Fluctuations on timescales less than 8-sec are essentially zero and the fluctuations are reduced for timescales of 64-sec and shorter. At longer time scales, though, the wavelet modes between the GHI point sensor and the simulation are essentially identical. The power plant output 'clear-sky index' agrees with the simulation results across all timescales (Fig. 5b).

B. Validation of Simulated Power plant Output

Here we present comparisons between the simulated and actual power output using the fluctuation power index (fpi) and ramp rate (RR) distributions. The fpi, which is the power content of fluctuations in the wavelet modes at each timescale, is used as a variability metric to test the WVM. The goal of the WVM is to create simulated power output that statistically has the same variability distribution across timescales as the actual power output. The main output of the WVM is the VR as a function of timescale, but small errors in VR are irrelevant if the fpi is small (such as on clear days or at very short timescales when fluctuations have tiny magnitudes), as
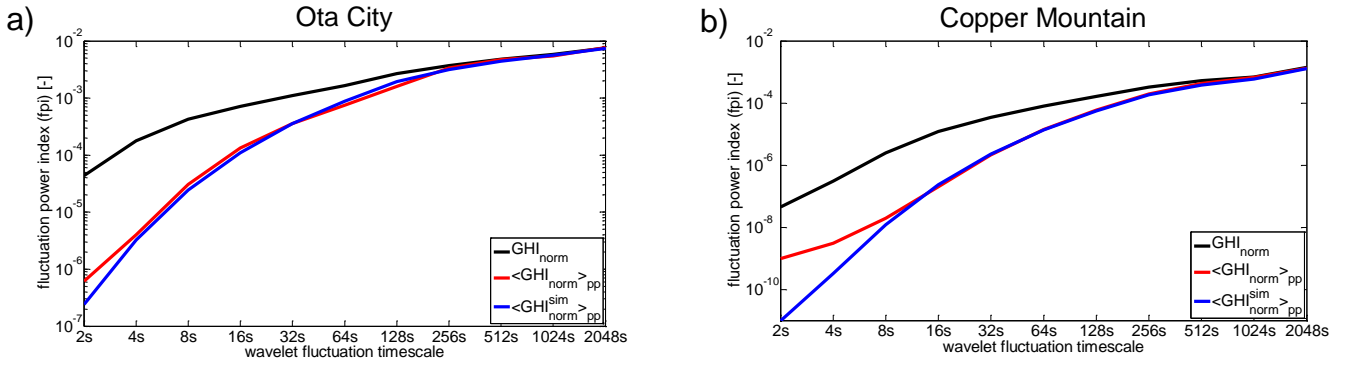
Fig. 6. Fluctuation power index (fpi) for the GHI point sensor (black), actual power output of (red), and simulated power output (blue line) at (a) Ota City on October 12, 2007 and (b) Copper Mountain on October 1, 2011.

errors will also be very small. However, when the fpi is large (such as on cloudy days or at long timescales), errors in VR can lead to significant errors in fpi. Additionally, GHI and total power output can be slightly offset in time based on the direction of cloud movement and the location of the GHI sensor versus the centroid of the power plant. Since the fpi describes the variability content (and total variance) rather than the time of occurrence, it allows measuring the accuracy of the WVM independent of these geographic limitations.

Fig. 6 shows the fpis of GHI_{norm}, $< GHI_{norm} >_{pp}$, and $< GHI_{norm}^{sim} >_{pp}$ for both OC and CM. As expected based on Fig. 5, the fpi of the irradiance at a point sensor, GHI_{norm}, deviates from the fpi of the spatial average, $< GHI_{norm} >_{pp}$, at short timescales due to geographic smoothing. There is good agreement between simulated and actual fpis of the power output 'clear-sky index' at all timescales. The variability at CM at timescales of 2 to 8-sec is higher than estimated by the WVM, though this may be caused by differences in sensor response times between the GHI and power measurements. Since the power content is so small at these timescales ($< 10^{-8}$ compared to $> 10^{-4}$ at longer timescales), though, there is little effect on simulated power output. At both sites, the WVM ($< GHI_{norm}^{sim} >_{pp}$) significantly improved over its input (GHI_{norm}) at quantifying the fluctuation power content of the actual power output .

Another validation of the model is to compare the irradiance profile of the input GHI point sensor, WVM output areal averaged irradiance, and the 'actual' area-averaged irradiance derived from the power output. To obtain the actual area-averaged irradiance, we multiply the power output clear-sky index by the GHI clear-sky model:

$$< GHI(t) >_{pp} = < GHI(t)_{norm} >_{pp} * GHI(t)_{clr}. \quad (11)$$

The simulated area-averaged irradiance clear-sky index must also be multiplied by the GHI clear-sky model to obtain simulated areal averaged irradiance:

$$< GHI^{sim}(t) >_{pp} = < GHI(t)_{norm}^{sim} >_{pp} * GHI(t)_{clr}. \quad (12)$$

Fig. 7 shows that $< GHI^{sim}(t) >_{pp}$ is essentially a filtered version of $GHI(t)$; during long clear or cloudy periods the area-averaged GHI approaches the point sensor while short fluctuations e.g., at 09:09, are more strongly reduced. The timeseries of fluctuations, $< GHI(t) >_{pp}$ and $< GHI^{sim}(t) >_{pp}$ are not expected to match perfectly, since only a single point sensor is used as input, but the statistics of the fluctuations are expected to agree. For the eight minute segment shown in Fig. 7a, the 'upper envelope' of area-averaged irradiance is accurately simulated. However, especially during long cloud events (large timescales), the lower envelope of the power plant is as small as or even smaller than the envelope of the point sensor. Physically this could mean that the optical depth of the cloud at the point sensor was less than the average of the cloud system over the power plant (spatial heterogeneity); it could also mean that the tilt and azimuth of the PV modules comprising the plant (versus the horizontal GHI) resulted in a smaller diffuse irradiance at the power plant during these morning hours.

While the WVM has been shown to match fpi (Fig. 6) and smoothing of area-averaged irradiance (Fig. 7), ramp rate statistics are often of greater interest to power plant and grid operators. Fig. 8 shows the cdf of ramp rates at 1s, 10s, 30s, and 1-min, for both OC and CM. P and P^{sim} show similar RR distributions at all of these timescales. The match between RRs is slightly worse at CM, but this is expected since CM is
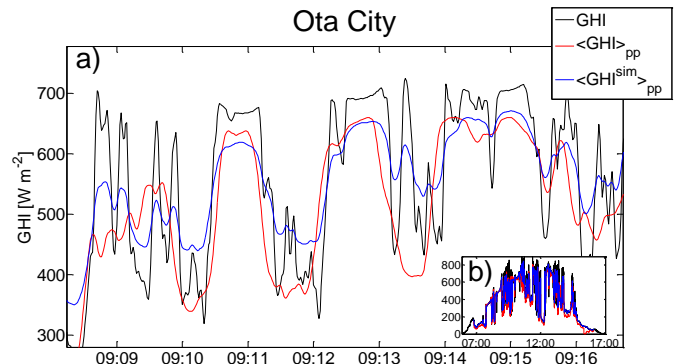

Fig. 7. Point sensor GHI (black), power plant area-averaged GHI (red), and simulated area-averaged GHI (blue) for Ota City on October 12, 2007. (a) Zoomed in to eight minutes in the morning, and (b) the entire day.
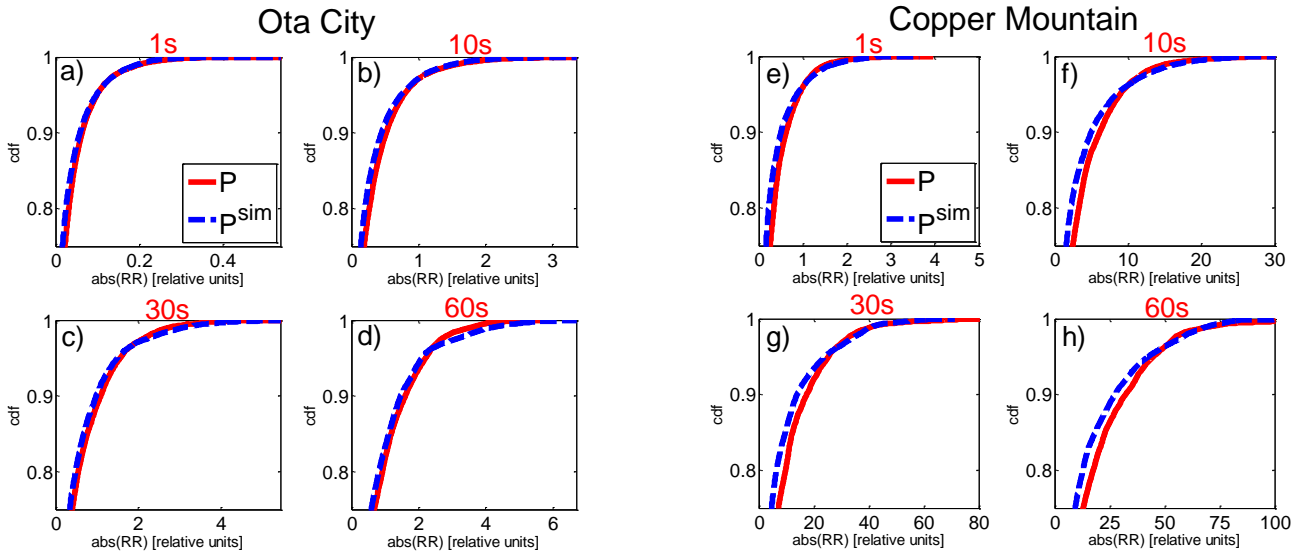
Fig. 8. Extreme (> **75** percentile) ramp rate distributions at 1-sec (a, e), 10-sec (b, f), 30-sec (c, g), and 1-min (d, h) for P and P^{sim} for Ota City (a-d) and Copper Mountain (e-h). X-axis units are multiplied by an arbitrary scaling factor to protect the confidentiality of the power data.

a larger area than OC. Over the larger area, the irradiance statistics may be less homogenous and lead to error in the WVM output. For example, half of CM could be consistently experiencing partly cloudy conditions while the other half is under clear skies. If the sensor used as input to the WVM were in the clear-sky section, the WVM would under predict the variability of the total plant. This scenario is less likely to happen at OC, since the distance across the plant is shorter (~1km at OC vs. ~2km at CM).

C. Comparison to Other Upscaling Methods

To evaluate the performance of the WVM, we compare it to other methods for simulating power plant output. We chose to compare to 3 other methods that have been applied for upscaling. (1) A primitive method is to simply linearly scale the irradiance measured by a single point sensor as $GHI \times CF$, where CF is a constant factor related to the plant area. This assumes identical relative variability between the point sensor and the whole plant, strongly overestimating variability for all but the smallest of PV plants. (2) Since geographic smoothing occurs over certain time scales (Fig. 5), a moving average (or box filter) can be applied to an irradiance timeseries. The timescale of the moving average can be physically motivated from the relation $t_{avg} = \frac{A^{1/2}}{V}$, where A is the plant area and V is the cloud velocity. While fundamentally similar to the WVM, this moving average method is restricted to smoothing at a single timescale (t_{avg}), and so cannot take into effect different amounts of smoothing at different timescales. (3) A third method is to average the timeseries from all available irradiance sensors. This method becomes more accurate as more sensors are added and in the extreme case of e.g. one sensor per PV panel would be exact. It requires the PV sensors to be representative of the actual plant layout: for best

results, sensors should be equally spaced and cover the entire plant footprint (but not extend past the footprint, or smoothing will be overestimated).

In Fig. 9, the extreme RRs of CM power output for these 3 methods are compared to the WVM on the test day. For method 2, the plant area is 1.33km, and a cloud speed of 10 m s^{-1} was assumed, resulting in a moving average timescale $t_{avg} = 115s$. For method 3, the 15 reference cells available at CM were averaged.

Method 1 overestimated the RRs at all timescales, since geographic smoothing is ignored. Method 2 also overestimated most RRs at all timescales (maximum RRs were underestimated), but performed markedly better than method 1. Method 2 could be improved by using measured cloud velocity instead of an assumed value. Method 3 overestimated RRs at shorter timescales (1s and 10s), but was more accurate at longer timescales (30s and 60s). At short timescales when short-distance changes are important, 15 sensors will not be enough to accurately represent all of the PV modules. As the timescale increases, the distances over which changes are important will increase, and this 15 sensor network will be more accurate in representing the entire plant.

Since grid operators are often concerned about worst-case scenarios, it is important that these simulation methods also produce reasonable maximum RRs. Table 2 shows the maximum RRs by timescale for each of the simulation methods. The WVM showed small percentage errors (-8% to -20%) at all timescales. Methods 1 and 3 will always overestimate the maximum RRs, since at 1 and 15 point measurements, respectively, they both underrepresent the actual diversity of the plant. As expected, Method 3 outperformed Method 1 with a range of errors of 8% to 38%.
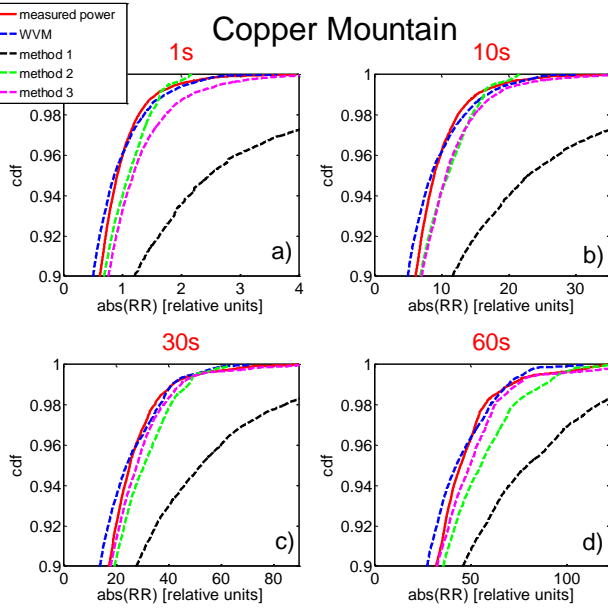
Fig. 9. Extreme (>90th percentile) ramp rate cumulative distribution functions at CM on October 1, 2011 at 1-sec (a), 10-sec (b), 30-sec (c), and 1-min (d) for measured power output (solid red), and for different methods of simulating PV power plant output: WVM (dashed blue), method 1: linearly scaling from a point sensor (dashed black), method 2: a moving average of 115s corresponding to $t_{avg} = \frac{A^{1/2}}{V}$ (dashed green line), and method 3: averaging all 15 reference cells (dashed magenta line).

Method 2, always overestimated the maximum RRs, and had moderate errors at most timescales (-0% to -45%).

Table 2: Maximum RRs for CM on the test day compared to maximum RRs simulated using other methods described in Section III.C. Relative units are used for RRs to protect confidential data.

		P	WVM	method 1	method 2	method 3
1s	max RR	0.50	0.46	4.08	0.28	0.68
	% error		-8%	723%	-45%	38%
10s	max RR	4.29	3.79	21.80	2.70	4.70
	% error		-12%	408%	-37%	9%
30s	max RR	11.19	8.92	24.95	7.88	12.11
	% error		-20%	123%	-30%	8%
60s	max RR	15.29	13.70	28.17	15.28	18.02
	% error		-10%	84%	-0%	18%

It is also worth noting the data requirements of each method. Aside from method 1 (which requires only a single sensor), the WVM has the simplest input requirements, needing just a single irradiance sensor and an A value. The A value can either be determined from a small network of irradiance sensors (~4-6), or reasonably estimated based on observed trends in A values. Method 2 requires the cloud velocity, which is difficult to determine since ground wind speeds are not well correlated with cloud speeds, and only sparse measurements exist of cloud height and winds aloft. Method 3 performs best with a high-density sensor network. When such a network is not available, the accuracy of method 3 will decrease towards that of method 1. Overall, the WVM has simple input requirements and is best at simulating extreme and maximum RRs.

IV. CONCLUSION

A wavelet-based variability model (WVM) for simulating the power output of a solar photovoltaic (PV) plant was presented and tested. The WVM uses the plant footprint, density of PV modules in the plant, and the timeseries measurements from a single point sensor to create a simulated power output timeseries. First, correlations between sites (i.e., houses or small groups of PV modules) within the power plant are determined using an equation based on the distance between sites, timescales, and a correlation scaling coefficient (A value). From these correlations, variability reductions (VRs), or the ratio of variability of a single point sensor to the variability of the entire PV plant, at each fluctuation timescale are found. Wavelet decomposition is then used to separate the normalized input point sensor timeseries by fluctuation timescale. By combining the wavelet modes at each timescale with the VRs at each timescale, the normalized plant power output is simulated. Actual power output (in MW) is then obtained by using a clear-sky model for power output.

The WVM was validated at the 2MW distributed residential rooftop plant in Ota City, Japan, and the Copper Mountain, NV 48MW central power plant. For both test cases, the WVM simulation matched the statistics of the actual power output well. Fluctuation power index (fpi) comparisons showed that the WVM accurately represented variability by timescale at both Ota City and Copper Mountain. Ramp rates (RRs) at 1-sec, 10-sec, 30-sec, and 60-sec were also compared between simulated and actual power, and again, the WVM fared well at both test sites.

Comparison between the WVM and other power plant simulation methods highlighted the benefits of using the WVM. The WVM has reasonable input requirements (single sensor and A value), while other methods required harder to obtain inputs such as cloud velocity or irradiance from a dense sensor network. The WVM was best at matching extreme and maximum RRs for the test day at Copper Mountain.

Future work will concentrate on characterizing the A values used in the correlation equation in section II.C. Currently, A values are determined form a small network of irradiance sensors. To allow for broader application of the WVM, we will determine how A values vary based on geographic region and meteorological condition. Then, a closed form WVM program will be created which will estimate the variability of potential PV plants for grid integration and siting studies without requiring a sensor network.

REFERENCES

[1] K. Otani, J. Minowa, and K. Kurokawa, "Study on areal solar irradiance for analyzing areally-totalized PV systems," *Solar Energy Materials and Solar Cells,* vol. 47, pp. 281-288, Oct 1997.

[2] A. E. Curtright and J. Apt, "The character of power output from utility-scale photovoltaic systems," *Progress in Photovoltaics,* vol. 16, pp. 241-247, May 2008.

[3] M. Lave and J. Kleissl, "Solar variability of four sites across the state of Colorado," *Renewable Energy,* vol. 35, pp. 2867-2873, Dec 2010.

[4] E. Wiemken, H. G. Beyer, W. Heydenreich, and K. Kiefer, "Power characteristics of PV ensembles: experiences from the combined power production of 100 grid connected PV systems distributed over the area of Germany," *Solar Energy,* vol. 70, pp. 513-518, 2001.

[5] A. Murata, H. Yamaguchi, and K. Otani, "A Method of Estimating the Output Fluctuation of Many Photovoltaic Power Generation Systems Dispersed in a Wide Area," *Electrical Engineering in Japan,* vol. 166, pp. 9-19, Mar 2009.

[6] A. Mills and R. Wiser, "Implications of Wide-Area Geographic Diversity for Short-Term Variability of Solar Power," *LBNL Report No. 3884E,* 2010.

[7] R. Perez, S. Kivalov, J. Schlemmer, K. Hemker, and T. Hoff, "Short-term irradiance variability: Station pair correlation as a function of distance," *Submitted to Solar Energy,* 2011.

[8] T. Hoff and R. Perez, "Modeling PV Fleet Output Variability," *Submitted to Solar Energy,* 2011.

[9] J. Marcos, L. Marroyo, E. Lorenzo, D. Alvira, and E. Izco, "From irradiance to output power fluctuations: the pv plant as a low pass filter," *Progress in Photovoltaics,* vol. 19, pp. 505-510, Aug 2011.

[10] P. Ineichen and R. Perez, "A new airmass independent formulation for the Linke turbidity coefficient," *Solar Energy,* vol. 73, pp. 151-157, 2002.

[11] M. Lave, J. Kleissl, and E. Arias-Castro, "High-frequency irradiance fluctuations and geographic smoothing," *Solar Energy*.

[12] J. Page, "The role of solar radiation climatology in the design of photovoltaic systems," in *Practical handbook of photovoltaics: fundamentals and applications*, T. Markvart and L. Castaner, Eds., ed Oxford: Elsevier, 2003, pp. 5-66.

[13] J. Boland, B. Ridley, and B. Brown, "Models of diffuse solar radiation," *Renewable Energy,* vol. 33, pp. 575-584, Apr 2008.

[14] C. Hansen, J. Stein, and A. Ellis, "Simulation of One-Minute Power Output from Utility-Scale Photovoltaic Generation System," 2011.

[15] D. King, W. Boyson, and J. Kratochvil, "Photovoltaic Array Performance Model," 2004.